Predicting lymphocyte dose and surviving fraction for VMAT and IMPT treatments with a dynamic lymphocyte flow model for locally advanced cervical cancer

C Kuipers, Sander; M van Tuyll van Serooskerken, Marianne; Lathouwers, Danny; Corbeau, Anouk; M de Boer, Stephanie; A Nout, Remi; S Hoogeman, Mischa; Godart, Jérémy

DOI
10.1088/1361-6560/ae0d29

Publication date
2025

Document Version
Final published version

Published in
Physics in medicine and biology

Physics in Medicine &
Biology

PAPER • OPEN ACCESS

Predicting lymphocyte dose and surviving fraction for VMAT and IMPT treatments with a dynamic lymphocyte flow model for locally advanced cervical cancer

To cite this article: Sander C Kuipers *et al* 2025 *Phys. Med. Biol.* **70** 215005

IOP Publishing Phys. Med. Biol. 70 (2025) 215005 https://doi.org/10.1088/1361-6560/ae0d29

Physics in Medicine & Biology

IPEM Institute of Physics and Engineering in Medicine

PAPER

Predicting lymphocyte dose and surviving fraction for VMAT and IMPT treatments with a dynamic lymphocyte flow model for locally advanced cervical cancer

Sander C Kuipers[1,2], **Marianne M van Tuyll van Serooskerken**[1,3], **Danny Lathouwers**[3], **Anouk Corbeau**[4], **Stephanie M de Boer**[4], **Remi A Nout**[1], **Mischa S Hoogeman**[1,2] **and Jérémy Godart**[1,2,*]

[1] Department of Radiotherapy, Erasmus MC Cancer Institute—University Medical Center Rotterdam, Rotterdam, The Netherlands
[2] Department of Medical Physics & Informatics, HollandPTC, Delft, The Netherlands
[3] Department of Radiation, Science and Technology, Delft University of Technlogy, Delft, The Netherlands
[4] Department of Radiation Oncology, Leiden University Medical Center, Leiden, The Netherlands
[*] Author to whom any correspondence should be addressed.

E-mail: j.schiphof-godart@erasmusmc.nl and s.c.kuipers@erasmusmc.nl

Keywords: lymphocyte flow model, locally advanced cervical cancer, radiation-induced lymphopenia, outcome prediction, lymphocyte sparing

OPEN ACCESS

RECEIVED
12 May 2025

REVISED
18 September 2025

ACCEPTED FOR PUBLICATION
29 September 2025

PUBLISHED
22 October 2025

Abstract

Objective. A dynamic model is developed to predict the impact of radiotherapy on circulating lymphocyte counts in women with locally advanced cervical cancer (LACC). This study aims to compare the effects of photon and proton therapy, as well as the influence of bone marrow sparing (BMS) techniques, on relative lymphocyte preservation over time. *Approach.* A dynamic lymphocyte flow model was developed to simulate the migration of lymphocytes based on seven compartments. Biological cell death and lymphocyte production were integrated across compartments. The lymphocyte flow model was applied to 19 LACC patients. Volumetric modulated arc therapy (VMAT) and intensity modulated proton therapy (IMPT) treatment plans were created for each patient without BMS and with BMS. The model calculated radiation dose to lymphocytes to estimate radiation-induced cell death over time. The output of the model was the relative lymphocyte count relative to baseline (RLC) over time and the RLC nadir in the blood and total body. *Main results.* According to the model, IMPT resulted in lower doses to lymphocyte and higher RLC nadirs compared to VMAT for all 19 patients. The total RLC nadir (mean $\pm$ SD) was 48.4% $\pm$ 4.0% for VMAT and 62.5% $\pm$ 5.1% for IMPT. In the blood compartment, the RLC nadir was 32.7% $\pm$ 3.5% for VMAT and 47.7% $\pm$ 5.9% for IMPT. The RLC nadir in the blood compartment improved with 3 Gy BMS from 32.7% $\pm$ 3.5% to 33.0% $\pm$ 3.5% , while it decreased for IMPT from 47.7% $\pm$ 5.9% to 46.6% $\pm$ 6.0%. Total RLC nadir decreased with BMS for VMAT from 48.4% $\pm$ 4.0% to 48.2% $\pm$ 3.9% and for IMPT from 62.5% $\pm$ 5.1% to 60.9% $\pm$ 5.3%. *Significance.* By incorporating a dynamic flow model, we predicted the RLC over time. The model predicted a substantial sparing effect IMPT has on the lymphocytes compared to VMAT. This sparing was both present in the blood and the total body. Sparing the bone marrow showed only a minimal effect on the RLC.

1. Introduction

The current standard treatment of locally advanced cervical cancer (LACC) is external-beam radiotherapy combined with cisplatin-based chemotherapy followed by brachytherapy (Cibula *et al* 2018, Pötter *et al* 2018). This treatment combination has shown to be highly effective with a very high locoregional control (Horeweg *et al* 2019, Pötter *et al* 2021). However, many patients undergoing this regimen develop lymphopenia (Wu *et al* 2016). There is increasing interest in adjuvant therapies that leverage the immune system to improve cancer treatment outcomes. This is reflected in trials investigating the

efficacy of immunotherapy in combination with chemoradiotherapy for the treatment of cervical cancer (Chung *et al* 2019, Colombo *et al* 2021, Monk *et al* 2023a, 2023b, Lorusso *et al* 2024). Furthermore, research has shown that radiation-induced lymphopenia (RIL) is associated with poorer overall survival in solid tumors, highlighting the need to better understand and mitigate the impact of radiotherapy on the immune system (Damen *et al* 2021).

For LACC, recent efforts have been made to spare lymphoid organs, including the bone marrow, during treatment planning for external-beam radiotherapy (EBRT) (Huang *et al* 2020). Bone marrow sparing (BMS) reduces the dose to the pelvic bones, therefore decreasing the risk of hematologic toxicities such as lymphopenia (Corbeau *et al* 2021a, Kuipers *et al* 2023). Another approach is proton therapy, which holds great promise to reduce the incidence of RIL for patients with LACC due to its potential sparing of lymphoid organs, such as the active bone marrow (Gort *et al* 2021, Kuipers *et al* 2024). For various other cancer types, namely oesophageal cancer, non-small cell lung cancer, and glioblastoma, the reduction in RIL by using protons instead of photons has been reported (Fang *et al* 2017, Shiraishi *et al* 2018, Routman *et al* 2019, Kim *et al* 2021, Mohan *et al* 2021, Li *et al* 2023, Cortiula *et al* 2024). While these immune-sparing strategies show the potential for reducing RIL by sparing lymphoid organs, quantifying the dose to lymphocytes and the risk of lymphopenia remains a challenge. This challenge arises because lymphocytes continuously circulate throughout the body, making it difficult to calculate their radiation exposure and predict RIL risk. Instead of focusing solely on sparing specific structures, a dynamic lymphocyte model can help account for temporal changes in immune cell distribution and improve predictions of RIL risk in individual patients. Previous studies have developed such models to correlate the EBRT dose to RIL (Jin *et al* 2017, 2020, Shin *et al* 2021). One of the most extensive models is the HEDOS-model, which is a time-dependent computational framework for calculating the dose to the circulating blood cells (Shin *et al* 2021). However, it solely considers the blood, which consists of 2% of the lymphocytes (Trepel 1974). The rest of the lymphocytes that are not in the peripheral blood are not considered. In a similar framework proposed by Jin *et al* (2020), RIL is modeled for patients with pancreatic ductal adenocarcinoma treated with radiotherapy by considering a dynamic model for lymphocyte migrating among 5 compartments of the immune system (Jin *et al* 2020). Developing a dynamic lymphocyte model for LACC patients would allow for a better understanding of the effect of immune-sparing strategies on the total lymphocyte count, and ultimately the development of individual immune system sparing approaches for women with LACC.

In this study, we build upon the model proposed by Jin *et al* (2020) and integrate it with the HEDOS model to capture lymphocyte dynamics in patients with LACC. Key adaptations include implementing a continuous residence-time function, combining short and long-residing compartments, and refining parameter estimation using equilibrium-state fitting. For this adapted model, we analyze the sensitivity of the model on the model parameters. Furthermore, we test the model to predict the difference in lymphocyte dose and surviving fraction between intensity-modulated proton therapy (IMPT) and volumetric-modulated arc therapy (VMAT) for these patients. Additionally, we asses with this model the impact of sparing the bone marrow with 3 Gy mean dose, a strategy during treatment planning aimed at reducing lymphocyte depletion by limiting the dose to active bone marrow, in lymphocyte surviving fraction.

2. Methods & materials

2.1. Lymphocyte compartmental model

A compartmental flow model comprising of seven compartments has been developed to simulate the migration of lymphocytes within the body. The model was taken and modified from the study of Jin *et al* (2020), which is based on the framework of Rannie and Ford (1978). Two extra compartments for the lymphoid organs were added, and no separate compartments were considered for the short-residing and long-residing lymphocytes. A schematic representation of our proposed model, with the seven compartments and the possible transitions between them, is shown in figure 1. The seven compartments in the model are the blood (B), lymph nodes (LN), red bone marrow (BM), skin (Sk), spleen (Sp), intestines (I), and other tissue (OT). The other tissue compartment consists of the lymphocytes in the rest of the body, which are mostly located in the mucosa of the respiratory tract. The intestines compartment is composed of the Peyer's patches and the intestinal mucosa (Trepel 1974).

Each compartment $i \in \{B, BM, Sp, LN, OT, Sk, I\}$ contains a number of lymphocytes $N_i(t)$ at time t which changes over time due to transitions, production, and cell death. The relative number of lymphocytes in equilibrium $N_i^{\text{eq}}/N_{\text{tot}}^{\text{eq}}$ were taken and adjusted from the study of Trepel (1974). Production of lymphocytes occurs in the lymph nodes, spleen, and bone marrow, while cell death is modeled in all compartments.

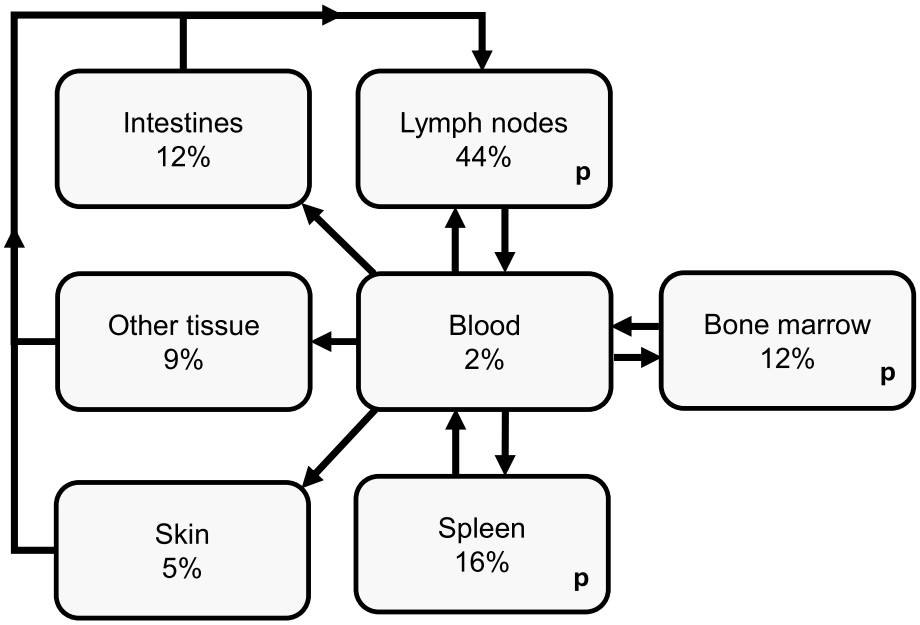

Figure 1. Schematic representation of the lymphocyte compartment model, representing the flow of lymphocytes between the seven compartments. The percentage indicates the fraction of lymphocytes present in each compartment in equilibrium. Compartments marked with 'p' indicate lymphoid organs where production is modeled. The model was taken and modified from the study of Jin *et al* (2020), which is based on the framework of Rannie and Ford (1978).

The transition dynamics between compartments are determined by flow probabilities $a_{i,j}$, which represent the probability of a lymphocyte moving from compartment i to j when it is leaving compartment i. The time until a lymphocyte leaves compartment i is governed by the residence-time probability density $p_i(t)$. This probability density is modeled as a combination of two Weibull distributions to make a distinction between short- and long-residing lymphocytes:

$$p_i(t) = w_i^{\mathrm{S}} p_i^{\mathrm{S}}(t) + \left(1 - w_i^{\mathrm{S}}\right) p_i^{\mathrm{L}}(t), \tag{1}$$

where $p_i^{\mathrm{S}}(t)$ and $p_i^{\mathrm{L}}(t)$ are the probability density functions (PDFs) of the short-residing and long-residing lymphocytes. The parameter w_i^{S} is the probability that a lymphocyte entering compartment i becomes short-residing in that compartment. The Weibull distribution in this model is described with a shape parameter of $k = 2$ and the scale parameter for the short and long-residing lymphocytes for compartment i, λ_i^{S} and λ_i^{L}, is defined by the average short and long-residing residence time, $\langle t_i^{\mathrm{S}} \rangle$ and $\langle t_i^{\mathrm{S}} \rangle$, respectively, such that the PDF for short and long-residing lymphocytes becomes:

$$p_i^{\mathrm{S,L}}(t) = \frac{2t}{\left(\lambda_i^{\mathrm{S,L}}\right)^2} \mathrm{e}^{-\left(\frac{t}{\lambda_i^{\mathrm{S,L}}}\right)^2}, \tag{2}$$

with $\lambda_i^{\mathrm{S,L}} = \langle t_i^{\mathrm{S,L}} \rangle / \Gamma(3/2) = 2\langle t_i^{\mathrm{S,L}} \rangle / \sqrt{\pi}$.

The probability of a lymphocyte going into apoptosis is independent of all factors. Every hour a lymphocyte has a probability of k_{ap} of going into apoptosis. Therefore, cell death is described with the PDF

$$p^{\mathrm{ap}}(t) = k^{\mathrm{ap}} \exp\left(-k^{\mathrm{ap}} t\right), \tag{3}$$

with k^{ap} the apoptosis rate. For lymphocyte production , we assume a constant production of Q lymphocytes per unit time in the lymph nodes, spleen, and bone marrow and no production in the rest of the compartments, such that the production in compartment i can be written as

$$Q_i = \begin{cases} Q & \text{for } i \in \{BM, LN, S\} \\ 0 & \text{otherwise.} \end{cases}$$

With the apoptosis, we can define the average effective time for long and short-residing lymphocytes $\langle t_{\mathrm{eff},i}^{\mathrm{S,L}} \rangle$ which is the residence time spent in a compartment before flowing to another compartment or

going into apoptosis. This average effective residence time is given by:

$$\left\langle t_{\mathrm{eff},i}^{\mathrm{S,L}} \right\rangle = \int_0^\infty \mathrm{d}t\, t \left(\frac{\pi\, t}{2\left\langle t_i^{\mathrm{S,L}} \right\rangle^2} \mathrm{e}^{-k^{\mathrm{ap}}t - \frac{\pi\, t^2}{4\left\langle t_i^{\mathrm{S,L}} \right\rangle^2}} + k^{\mathrm{ap}}\, \mathrm{e}^{-k^{\mathrm{ap}}t - \frac{\pi\, t^2}{4\left\langle t_i^{\mathrm{S,L}} \right\rangle^2}} \right). \tag{4}$$

The derivation of this expression is presented in appendix A.

This average residence time can be derived with the apoptosis rate k^{ap} and the residence-time PDFs $p_i^{\mathrm{S,L}}(t)$ that are described by the average long- or short-residing time $\langle t_i^{\mathrm{S,L}} \rangle$. To find the value for the percentage of lymphocytes that becomes short residing, introduced in equation (1), we define the equation for the fraction of lymphocytes that is short residing in equilibrium:

$$f_i^{\mathrm{S}} = \frac{N_i^{\mathrm{eq,S}}}{N_i^{\mathrm{eq,L}} + N_i^{\mathrm{eq,S}}}, \tag{5}$$

with $N_i^{\mathrm{eq,S}}$ and $N_i^{\mathrm{eq,L}}$ the number of lymphocytes in equilibrium in compartment i that is short or long residing. With this equation, we can obtain a definition of the short-residing weight w_i^{S} in terms of the average effective residence times and the fraction of short residing lymphocytes in equilibrium:

$$w_i^{\mathrm{S}} = \frac{f_i^{\mathrm{S}} \langle t_{\mathrm{eff},i}^{\mathrm{L}} \rangle}{\left(1 - f_i^{\mathrm{S}}\right) \langle t_{\mathrm{eff},i}^{\mathrm{S}} \rangle + f_i^{\mathrm{S}} \langle t_{\mathrm{eff},i}^{\mathrm{L}} \rangle}. \tag{6}$$

The full derivation of this equation is substantiated in appendix B.

To obtain the population-average equilibrium state, we define the removal rate $k_i^{\mathrm{re}} = \langle t_{\mathrm{eff},i} \rangle^{-1}$, where $\langle t_{\mathrm{eff},i} \rangle = w_i^{\mathrm{S}} \langle t_{\mathrm{eff},i}^{\mathrm{S}} \rangle + (1 - w_i^{\mathrm{S}}) \langle t_{\mathrm{eff},i}^{\mathrm{L}} \rangle$. At equilibrium the lymphocyte balance in compartment i is

$$\sum_j a_{j,i} \left(k_j^{\mathrm{re}} - k^{\mathrm{ap}} \right) N_j^{\mathrm{eq}} - k_i^{\mathrm{re}} N_i^{\mathrm{eq}} + Q_i = 0, \tag{7}$$

where k^{ap} is the rate of apoptosis per unit time, Q_i is the number of lymphocytes produced in compartment i per unit time, and $a_{i,j}$ is the probability of a lymphocyte flowing from compartment i to j. From figure 1, it follows that only 12 values of $a_{i,j}$ in the 7×7 flow probability matrix are non-zero in our model. Specifically, $a_{LN,B}, a_{BM,B}, a_{S,B}, a_{Sk,LN}, a_{OT,LN}$, and $a_{I,LN}$ are 1, while $a_{B,LN}, a_{B,BM}, a_{B,OT}, a_{B,Sk}, a_{B,I}$, and $a_{B,Sp}$ are undetermined. The equilibrium condition is considered for the estimation of the initial parameter values. By solving these equations, the equilibrium constraints can be obtained for this model. The derivation of these constraints is outlined in appendix C.

2.2. Modeling lymphocyte flow

The compartmental model was implemented in discrete time using a particle-based approach. Each lymphocyte was represented as an entry in two vectors: one tracking the current compartment of each lymphocyte and the other storing the remaining residence time for each lymphocyte in its compartment. At each time step Δt, the algorithm proceeded as follows:

(i) Transition: For lymphocytes with a remaining residence time of zero, the transition matrix $a_{i,j}$ was used to determine the next compartment. New remaining residence times for the lymphocytes are sampled based on the derived residence time distribution of the new compartment $p_i(t)$.
(ii) Cell death: Lymphocytes underwent apoptosis probabilistically, based on the apoptosis rate k^{ap} and the PDF defined in equation (3).
(iii) Lymphocyte creation: New lymphocytes were created in designated compartments based on the creation parameter Q. The new lymphocytes were assigned an initial residence time based on the residence time probability distributions of their respective compartments.
(iv) Residence time update: For all surviving lymphocytes, the remaining residence times were decremented by the time step size Δt.

This approach stochastically models the transitions, apoptosis, and lymphocyte creation. To analyze the model output, the positions of all lymphocytes were recorded at regular intervals $\Delta t_{\mathrm{output}}$ and stored for further analysis. This output was used in the next part of the model to compute the dose to the lymphocytes.

2.3. Radiation dose to lymphocytes

The radiation dose to the lymphocytes was calculated based on the recorded compartmental positions at the EBRT fraction time points t_{EBRT}. Dose probability distributions for each compartment were derived using delineations on patient planning CT scans and the dose distribution from treatment plans. The derivation of these distributions is detailed in section 2.5. At fraction time points, the dose for each lymphocyte was sampled from these distributions. If a lymphocyte remained in the same compartment until the next fraction time point and the lymphocyte was not in the blood compartment, the same dose was sampled for the consecutive fraction time point. This approach enabled the creation of a dose-volume histogram (DVH) for the lymphocytes per treatment day and for the whole treatment. To estimate the lymphocyte survival, we applied a linear survival model $S(D) = \mathrm{e}^{-\alpha D}$, with D the dose and α a radiosensitivity constant. In our model, a radiosensitivity of $\alpha = 0.4\,\mathrm{Gy}^{-1}$ was used (Paganetti 2023). Because the lymphocytes are not affected by fractionation in a linear survival model, the cumulative dose was applied to calculate the surviving fraction at each time point. Furthermore, newly produced lymphocytes enter with zero dose and then accumulate dose according to their compartmental locations, while lymphocytes removed by natural apoptosis are withdrawn from the calculations for the cumulative dose.

2.4. Patient data and treatment plans

This study retrospectively included 19 women treated with primary chemoradiotherapy and concurrent chemotherapy for LACC according to the EMBRACE-II protocol at Erasmus MC between December 2019 and January 2021 (Pötter *et al* 2018). The patient cohort, planning CT scans, and delineations were identical to that of the study of Kuipers *et al* (2023). For these patients, four treatment plans were evaluated. Two VMAT treatment plans were obtained from this earlier study, namely one with no BMS objective in the treatment planning, and one incorporating a planning objective aimed at reducing the mean bone marrow dose by 3 Gy (Kuipers *et al* 2023). For the IMPT treatment plans, we used the treatment plans without BMS and with 3 Gy mean dose BMS for these patients as described in the study of Kuipers *et al* (2024). The outer contour of the pelvic bones was taken as a surrogate for the active bone marrow as this delineation has been shown to be most predictive of hematologic toxicity in women with LACC (Corbeau *et al* 2021a). All treatment plans were designed for 25 fractions of 1.8 Gy with 5 fractions per week. The planning constraints of all plans adhered to the EMBRACE-II protocol (Pötter *et al* 2018). A detailed description of the patient cohort, target and normal tissue delineation, treatment planning methodology, and dose parameters is provided in the two referenced studies (Kuipers *et al* 2023, 2024).

2.5. Radiation dose to the compartments

For estimating the patient-specific lymphocyte dose, the location of each lymphocyte at the start of each fraction was used with the corresponding dose probability distribution of its compartment. Lymphocyte movement between compartments during the beam-on time was not taken into account. Dose probability distributions were derived from patient-specific planning CT scans, delineations, and dose distributions.

For the bone marrow, the outer contour of the pelvic bones were delineated from the inferior level of the ischial tuberosities to 2 cm superior to the planning target volume of the patient. With this delineation, every part of the bone marrow that receives significant dose is taken into account. The relative number of lymphocytes that is in this structure is obtained from the study of Ellis (1961). In our patient cohort, the internal iliac, external iliac, obturator, presacral, and the common iliac region nodes are included in the elective clinical target volume (CTV-E). These nodes represent an estimated 6% of the total number of lymph nodes (Panici *et al* 1992, Qatarneh *et al* 2006, Kim *et al* 2020). If the patient was identified as a high-risk patient, the paraaortic lymph nodes are also included in the CTV-E, which increases the fraction of lymph nodes in the CTV-E to 11% (Panici *et al* 1992). The mesenteric nodes are also irradiated and consist of approximately 54% of all the lymph nodes in a human body (Kim *et al* 2020). To estimate the dose to the mesenteric lymph nodes, the DVH for the small bowel bag was taken as a substitute. The small bowel bag was delineated until 2 cm above the planning target volume, therefore a distinction was made between medium- and high-risk patients. In our model, we assumed that 50% of the mesenteric lymph nodes were located within the delineated small bowel bag for medium-risk patients, while this fraction increased to 70% for high-risk patients. For the intestines compartment, the small bowel delineation was taken as a substitute. The Peyer's patches are mostly situated in the last part of the small bowel, therefore, we assumed all Peyer's patches to be within the delineated small bowel bag. For the skin compartment, an outer contour of the body of 2 mm of the pelvis was delineated on the CT scan. Following the study of Shin *et al* (2021), the relative volume of skin in the pelvis was set to 13.8%. The spleen and other-tissue compartments were assumed to receive no dose for patient with LACC.

For the blood compartment, we used the HEDOS model (Shin *et al* 2021), a computational tool designed to calculate the dose received by circulating blood cells during EBRT. The HEDOS model simulates the blood flow network. We adapted the model to include the cervix–uterus as a blood flow compartment. The blood flow to the cervix–uterus was estimated to be 1.4% of the cardiac output (Page and Rollins 2019), and its blood content was set to 0.05% of the total blood volume (Kim *et al* 2020). Anatomically, the uterus was positioned in the model's flow network receiving blood from large arteries and draining into large veins. For dose calculations, patient-specific DVHs were used as input to the HEDOS simulation. Beam-on times were set to reflect delivery differences between treatment modalities: 4 min per fraction for VMAT and 12 min per fraction for IMPT.

2.6. Parameter optimization

The set of model parameters are stated in table 1. The reference values for most parameters in the model were based on literature. For parameters that lacked reported values, the average was taken of analogous parameters with reported values in the literature. The reference values for the parameters are also listed in table 1. A substantiation and discussion for the reference values of the parameters is given in appendix D. While these reference values provide a starting point, they must satisfy the equilibrium constraints derived in appendix C. To address this, we define a quadratic loss function that minimizes the discrepancies between some of the model parameters and their reference values while incorporating the flow equations and equilibrium constraints.

To estimate the model parameters, we defined a quadratic loss function such that the difference between the model parameters γ_j and the reference values of the parameters γ_j^{lit} is minimized:

$$L = \sum_j \left(\beta_j \frac{\gamma_j - \gamma_j^{\text{lit}}}{\gamma_j^{\text{lit}}} \right)^2, \tag{8}$$

where β_j is a weight for the certainty of the reference value. The weights for each parameter are stated in table 1. Each term is normalized by $(\gamma_j^{\text{lit}})^{-2}$ to ensure that the optimization process does not disproportionately prioritize parameters with larger values. We fix N_i^{eq}, f_i^{S}, and $\langle t_i^{\text{L}} \rangle$ to their reference values. For the rest of the variables, i.e. $\langle t_i^{\text{S}} \rangle$, k^{ap}, Q_i, and $a_{i,j}$, the difference is minimized with this function. The removal rate k_i^{re} is taken as a substitute for $\langle t_i^{\text{S}} \rangle$ in the loss equation and its reference value is calculated with equation (4) and using that k_i^{re} is the inverse of $\langle t_{\text{eff},i} \rangle$.

By incorporating the equilibrium constraints derived in appendix C, we demonstrated that eight parameters, γ_k, are not independent but instead depend on the remaining parameters, γ_l, through a known relationship, $\gamma_k = g_k(\{\gamma_l\})$. Substituting this dependency directly into the loss function reduces the number of independent parameters, thereby decreasing the dimensionality of the optimization problem and ensuring that the model inherently respects the equilibrium constraints.

$$L = \sum_{\gamma_l} \left(\beta_l \frac{\gamma_l - \gamma_l^{\text{lit}}}{\gamma_l^{\text{lit}}} \right)^2 + \sum_{\gamma_k} \left(\beta_k \frac{\gamma_k(\{\gamma_l\}) - \gamma_k^{\text{lit}}}{\gamma_k^{\text{lit}}} \right)^2. \tag{9}$$

The parameters γ_k corresponds to the parameters k_i^{re} for $i \in \{BM, Sp, LN, OT, Sk, I\}$, Q, and $a_{B,I}$. These parameters are related to the other parameters γ_l by the equilibrium constraints. γ_l consists of the parameters k_i^{re} for all i, $a_{B,i}$ for $i \in \{BM, S, LN, OT, Sk\}$, k^{ap}, and k_1^{re}. By minimization of this loss function in terms of γ_l, the resulting values are as close as possible to their reference values while adhering to the flow equations in equilibrium. Next, as the removal rate k_i^{re} was taken as a substitute for $\langle t_i^{\text{S}} \rangle$ in the loss equation, we obtained the $p_i^{\text{S}}(t)$ as we fixed f_i^{S} and $\langle t_i^{\text{L}} \rangle$ to its reference values.

2.7. Analysis

In this study, the model was run with $\Delta t = 0.1$ h and $N = 10^7$. The treatment was given in 25 fractions, with 24 h intervals in between and 72 h after every fifth fraction, to simulate the weekends. For the comparison between IMPT and VMAT, the treatment plans without BMS for both IMPT and VMAT are used. The primary outcomes of the lymphocyte flow model included the relative lymphocyte count (RLC) over time, which represents the lymphocyte count normalized to its baseline (or equilibrium) level, and the RLC nadir in both the blood and the total body. Moreover, the DVH of the lymphocytes after the last fraction was determined. For studying the effect of BMS, the RLC of the treatment plans without BMS and with 3 Gy BMS are compared for both VMAT and IMPT. The mean value for all patients is reported as well as the standard deviation which expresses the inter-patient variability.

To assess the statistical uncertainty of the model for a single run with $N = 10^7$ lymphocytes, the model was executed 10 times for a single treatment plan. This treatment plan was the no BMS VMAT

Table 1. The reference values for the different parameters for the lymphocyte flow model. The weight β_j is used in the quadratic loss minimization in equation (8). B = blood; LN = lymph nodes; BM = bone marrow; Sk = skin; Sp = spleen; I = intestines; OT = other tissue; N_i^{eq} = number of lymphocytes in equilibrium; $\langle t_i^{\mathrm{S}} \rangle$ = average short-residence time; $\langle t_i^{\mathrm{L}} \rangle$ = average long-residence time; f_i^{S} = fraction short-residing lymphocytes; k^{ap} = apoptosis rate; Q = lymphocyte production; $a_{B,i}$ = flow probability from blood compartment to i.

Parameter	Compartment	Lit value	Weight β_j	References
N_i^{eq}	B	$1 * 10^{10}$	N.A.	Trepel (1974)
	LN	$19 * 10^{10}$	N.A.	Trepel (1974)
	BM	$5 * 10^{10}$	N.A.	Trepel (1974)
	Sk	$2 * 10^{10}$	N.A.	Trepel (1974)
	Sp	$7 * 10^{10}$	N.A.	Trepel (1974)
	I	$5 * 10^{10}$	N.A.	Trepel (1974)
	OT	$4 * 10^{10}$	N.A.	Trepel (1974)
$\langle t_i^{\mathrm{S}} \rangle$	B	0.5 h	1/2	Westermann and Pabst (1992)
	LN	16.5 h	1	Rannie and Ford (1978), Ford (1979)
	BM	2.5 h	1	Rannie and Ford (1978), Ford (1979)
	Sk	8 h	1/4	
	Sp	4.5 h	1	Rannie and Ford (1978), Ford (1979)
	I	8 h	1/4	
	OT	8 h	1/4	
$\langle t_i^{\mathrm{L}} \rangle$	All	1440 h	N.A.	
f_i^{S}	B	0.6	N.A.	Young *et al* (1997)
	All except B	0.2	N.A.	
k^{ap}	N.A.	$4.3 * 10^{-5}$ h^{-1}	1/2	Lutz *et al* (2011), Sender and Milo (2021)
Q	N.A.	$6.1 * 10^{6}$	1/2	Lutz *et al* (2011), Sender and Milo (2021)
$a_{B,i}$	LN	0.18	1	Rannie and Ford (1978), Ford (1979)
	BM	0.15	1	Rannie and Ford (1978), Ford (1979)
	Sk	0.03	1/4	
	Sp	0.55	1	Rannie and Ford (1978), Ford (1979)
	I	0.04	1/2	Ford (1979)
	OT	0.05	1/4	Ford (1979)

treatment plan of Patient 1. The standard deviation of the nadir values over these runs was taken as the per-run uncertainty.

The deviation from reference value after parameter optimization was determined. Additionally, a sensitivity analysis was performed on the relative number of lymphocytes per compartment N_i/N_{tot}, the average short residence time $\langle t_i^{\mathrm{S}} \rangle$, the average long residence time $\langle t_i^{\mathrm{L}} \rangle$, the relative number of short-residing lymphocytes in equilibrium f_i^{S}, the outflow probability $a_{B,i}$, the apoptosis rate k^{ap}, the production c, and the radiosensitivity α. Every variable x was shifted with $\Delta x = 10\%$ and the sensitivity index was measured in terms of the shift in lymphocyte nadir in the body:

$$SI = \frac{y(x+\Delta x) - y(x-\Delta x)}{2\Delta x}, \tag{10}$$

where y is the nadir in the body. The runs for the sensitivity analysis were done with $N = 10^6$.

The evaluation of the dose, lymphocyte count, and the sensitivity analysis was done in Matlab 2021b.

Table 2. Optimized parameters and their percentage deviations from the reference values obtained with the quadratic loss function stated in equation (8).

Parameter	Compartment	Exp value	Optimized value	Deviation
$\langle t_i^S \rangle$	*B*	0.5 h	0.7 h	34%
	LN	16.5 h	13.6 h	−18%
	BM	2.5 h	4.6 h	85%
	Sk	8.0 h	13.8 h	72%
	Sp	4.5 h	3.7 h	−18%
	I	8.0 h	24.5 h	206%
	OT	8.0 h	23.0 h	187%
k^{ap}	N.A.	$4.3 * 10^{-5}$ h^{-1}	$4.3 * 10^{-5}$ h^{-1}	0.08%
Q	N.A.	$6.1 * 10^{6}$ h^{-1}	$6.1 * 10^{6}$ h^{-1}	0.08%
$a_{B,i}$	*LN*	0.18	0.20	12%
	BM	0.15	0.24	63%
	Sk	0.03	0.03	13%
	Sp	0.55	0.43	−22%
	I	0.04	0.05	17%
	OT	0.05	0.04	23%

3. Results

The optimization of parameters using a quadratic loss function resulted in deviations from their expected values. Table 2 presents the optimized values along with the percentage deviations from their expectations. Notably, the largest deviations were observed in the short residence time for the intestines compartment (206%) and the other tissue compartment (187%). In contrast, the creation parameter (Q) and apoptosis parameter (k^{ap}) showed minimal deviations of only 0.08%. Among the flow probabilities, all increased except for the probability of flow from the blood compartment to the spleen.

The dose (mean ± SD) to the lymphocytes was 6.7 ± 1.0 Gy for the VMAT treatment and 4.4 ± 0.9 Gy for the IMPT treatment. In figure 2, the average DVH is shown for VMAT and IMPT. For VMAT, the amount of lymphocytes that received no dose (mean ± SD) was 31.5% ± 2.1%, whereas this was 41.5% ± 4.4% for the IMPT treatment. The difference in dose resulted in a substantial difference in the lymphocyte count, favorable for the IMPT treatment. Relative lymphocyte counts for VMAT and IMPT are compared in figure 3, both for the total lymphocyte count and the blood compartment. Weekends were distinctly observable, as lymphocyte counts did not decrease due to the absence of treatment. The nadir in the blood compartment was consistently lower than the total nadir. The total relative lymphocyte nadir (mean ± SD) was 48.4% ± 4.0% for VMAT and 62.5% ± 5.1% for IMPT. In the blood compartment, the nadir was 32.7% ± 3.5% for VMAT and 47.7% ± 5.9% for IMPT. The differences between IMPT and VMAT for both nadirs were statistically significant ($p < 10^{-3}$).

The RLC nadir in both the blood compartment and in total was compared between VMAT and IMPT under two BMS scenarios: 0 Gy and 3 Gy BMS. In figure 4, this comparison is illustrated for the blood compartment and in total. In the blood compartment, the RLC nadir for VMAT improved from 32.7% ± 3.5% (mean ± SD) for 0 Gy sparing to 33.0% ± 3.5% for 3 Gy sparing ($p < 10^{-3}$), while for IMPT, the nadir decreased when introducing 3 Gy BMS from 47.7% ± 5.9% to 46.6% ± 6.0% ($p < 10^{-3}$). For VMAT, the total RLC nadir decreased from 48.4% ± 4.0% for 0 Gy sparing to 48.2% ± 3.9% for 3 Gy sparing ($p = 0.016$) and for IMPT it decreased from 62.5% ± 5.1% to 60.9% ± 5.3% for BMS.

To assess statistical variability, we computed the nadir for a single treatment plan over 10 runs with different random seeds. This showed a mean ± SD of 0.5078 ± 0.0001 for the body nadir, corresponding to a relative uncertainty of 0.02%, and 0.3656 ± 0.0009 for the blood nadir, corresponding to a relative uncertainty of 0.2%. These values indicate that stochastic noise of the model with $N = 10^7$ lymphocytes has negligible impact on the reported nadirs and that the variation in the reported nadirs resulted from the variation in treatment plans.

Figure 5 illustrates the sensitivity analysis results for 35 parameters, with each boxplot representing data from 38 treatment plans. The highest sensitivity was associated with the number of lymphocytes in each compartment (N_i), revealing that an increase in lymphocytes within irradiated compartments leads to a lower lymphocyte nadir, and vice versa. Additionally, the fraction lymphocytes that is short residing (f_i^S) showed notable sensitivity, particularly in the lymph nodes compartment. The average long-residence time also displayed relatively large sensitivity in the lymph nodes compartment. In contrast, the average

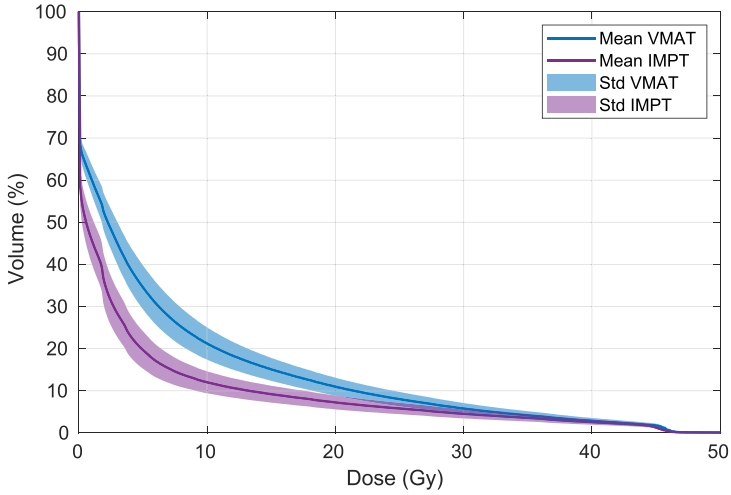

Figure 2. The dose-volume histogram for the lymphocytes at the end of the treatment for VMAT and IMPT.

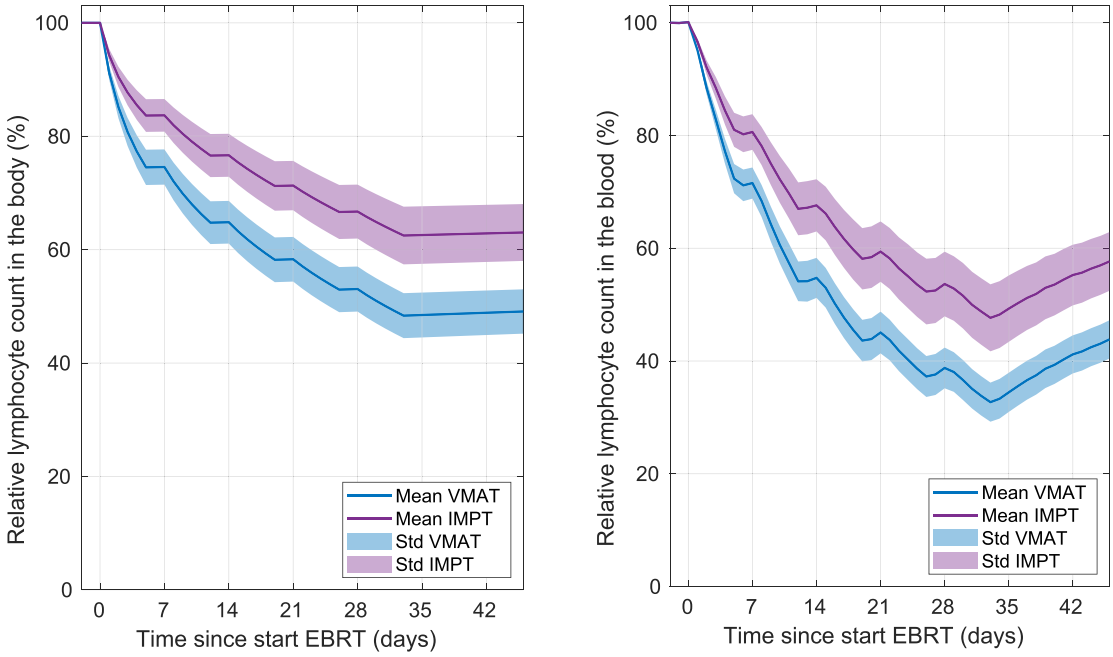

Figure 3. Relative lymphocyte count per day in total (left) and in the blood compartment (right) as a function of time since start of the external-beam radiotherapy for VMAT (blue) and IMPT (purple).

short-residence time, flow probabilities, and the creation and apoptosis rates demonstrated low sensitivity, with $SI < 0.02$. For the parameters f_s^{Sk}, t_s^{BM}, t_s^{S}, t_s^{OT}, t_s^{Sk}, t_s^{I}, $a_{B,BM}$, $a_{B,S}$, $a_{B,LN}$, $a_{B,OT}$, $a_{B,Sk}$, k^{ap}, and Q, the variation followed predominantly from the statistical variability. For the rest of the parameters, the variability resulted from the variation in treatment plans.

4. Discussion

In this research, a compartmental model was developed to model the lymphocyte flow and predict the EBRT dose to lymphocytes and the lymphocyte count in the context of the treatment of LACC. This model enabled us to study the impact of immune-sparing strategies on the lymphocyte dose and count. Our results showed that IMPT delivers lower doses to circulating lymphocytes compared to VMAT, highlighting its potential to better protect the immune system during treatment. These findings suggest that IMPT better preserves the lymphocytes and the immune system, which is critical for patient outcomes. Furthermore, the expected benefit for introducing 3 Gy BMS in the treatment planning was shown to

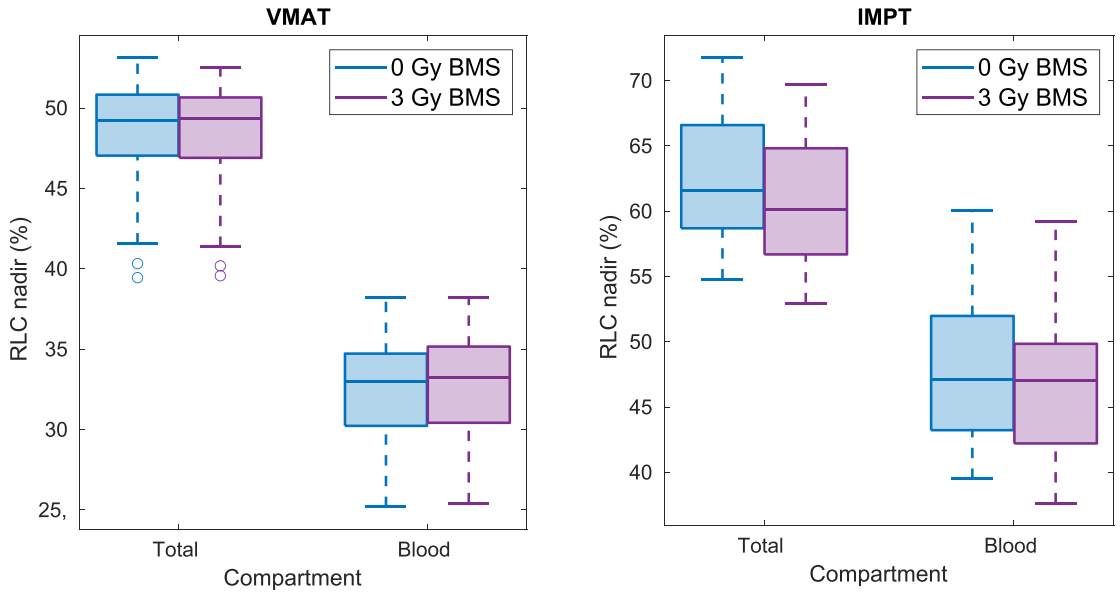

Figure 4. Boxplots of the relative lymphocyte count (RLC) nadir for VMAT (left) and IMPT (right) for 0 Gy bone marrow sparing (blue) and 3 Gy bone marrow sparing (purple) in total and in the blood compartment.

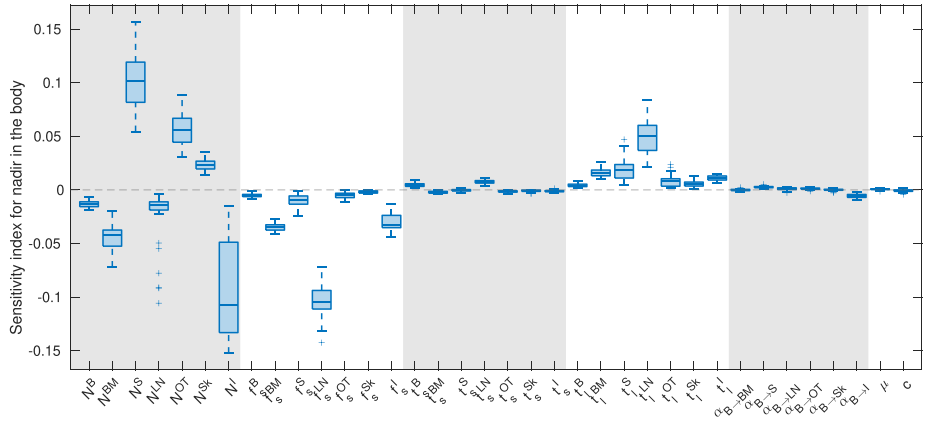

Figure 5. Sensitivity index for 35 input parameters for the lymphocyte flow model. Every boxplot consists of 19 VMAT plans and 19 IMPT plans. The gray and white boxes group the different kind of parameters.

have only a small positive effect for VMAT on the lymphocyte count and have a minimal negative effect for IMPT on the lymphocyte count.

Given the correlation between RIL and poorer prognoses for overall survival, sparing lymphocytes could positively impact treatment outcomes (Damen *et al* 2021). Our model shows a very evident lymphocyte sparing with proton therapy compared to the conventional photon therapy. The mean dose to the lymphocytes was reduced with 2.3 Gy on average, from 6.7 Gy to 4.4 Gy. This reduction resulted in a substantial improvement in relative lymphocyte count nadir for proton therapy with 63% compared to 48% for photon therapy in the body and RLC nadir was 33% for VMAT and 48% for IMPT. Clinical trials, such as the PROTECT trial, are needed to confirm whether the predicted lymphocyte-sparing benefits of proton therapy observed in our model (Corbeau *et al* 2021b) translate into actual improvements for patients with LACC (Corbeau *et al* 2021b). For other treatment sites, the potential to spare the immune system with proton therapy compared to photon therapy has already been shown in several clinical studies (Fang *et al* 2017, Shiraishi *et al* 2018, Routman *et al* 2019, Kim *et al* 2021, Mohan *et al* 2021, Li *et al* 2023).

Sparing the bone marrow in treatment planning is a potential strategy to reduce the incidence of hematologic toxicities, including RIL (Huang *et al* 2020, Corbeau *et al* 2021a). However, our lymphocyte flow model demonstrated minimal dosimetric benefit for lymphocyte survival when comparing 3 Gy BMS to standard treatment plans. Notably, for proton therapy, BMS seems to worsen the lymphocyte

count, as the reduced dose to the bone marrow often comes at the expense of increased dose to other organs at risk (Kuipers *et al* 2024). Although clinical studies have reported reductions in hematologic toxicity with BMS in photon therapy, our model did not reproduce this effect. This discrepancy could be caused by our model focusing on the dose to circulating lymphocytes and it does not include bone marrow suppression, which can be radiation induced. Future modeling efforts could expand on this by incorporating aspects of bone marrow function and regeneration.

In our model, blood lymphocyte counts did not mirror the total body lymphocyte pool. Across all treatment plans, the blood nadir was lower than the total body nadir. This could be because of the non-uniform radiation exposure and the transient state that will follow before returning to equilibrium. Taking this into account could be clinically relevant, as blood lymphocyte counts are often used as a surrogate for overall immune status.

In this study, we have performed a sensitivity analysis of our lymphocyte flow model on 35 parameters using data from 38 treatment plans, as illustrated in figure 5, to understand which parameters are most important. The analysis showed that the model output was most impacted by the number of lymphocytes in each compartment (N_i), as this showed the highest sensitivity index. Specifically, a relative increase in lymphocytes within irradiated compartments resulted in a lower lymphocyte nadir, while a decrease produced the opposite effect. Notably, the fraction of short-residing lymphocytes (f_i^S) and the average long-residence time displayed considerable sensitivity, particularly within the lymph nodes compartment. A smaller fraction of long-residing lymphocytes or shorter long-residence times increases the flow of lymphocytes through the irradiation field, thereby exposing more lymphocytes to dose and lowering their survival probability. In contrast, parameters such as the average short-residence time, flow probabilities, and rates of lymphocyte creation and apoptosis demonstrated low sensitivity, with $SI < 0.02$. Obtaining accurate values for parameters with high sensitivity indices is more important for this model to obtain a more reliable prediction.

Our model considers the dynamics of lymphocytes and predicts the dose to lymphocytes during EBRT. It is an adaptation of the framework proposed by Jin *et al* (2020), with significant modifications and the integration of the HEDOS model to predict the dose to lymphocytes in the blood (Shin *et al* 2021). Our adaptations and improvements address some of the limitations of the original model and enhance its predictive capabilities. First, we implemented a continuous residence-time function based on a Weibull distribution to model the lymphocyte residence time within organs and the bloodstream. Additionally, the effect of radiation-induced cell death and the distinction between long and short-residing lymphocytes was incorporated directly into this function. Furthermore, we addressed the gaps in the literature regarding key parameters by relying on available data and fitting this data to the equilibrium state.

Recent work of de Kermenguy *et al* (2024) and Beekman *et al* (2025) have both explored lymphocyte dynamics in the context of radiotherapy by creating a compartmental lymphocyte flow model combining short transition times of the blood flow and longer transitions time for the flow through lymphoid organs. While these studies provide valuable insights, they are methodologically distinct from our approach. Both studies did not account for lymphocyte creation/annihilation or tissue-resident lymphocytes. The study of de Kermenguy *et al* (2024) focused on brain tumors and out-of-field doses, without taking into account the bone marrow as an compartment in their model. Furthermore, they did not solve the equilibrium equations and only used literature values for the transition parameters and not the equilibrium distribution of lymphocytes. The study of Beekman *et al* (2025) focussed exclusively on mice and did not attempt to bridge their findings to humans. By incorporating tissue-resident lymphocytes, dynamic lymphocyte creation/annihilation, and an application to cervical cancer, our model provides a different framework for understanding lymphocyte dynamics in radiotherapy.

The model developed in this study might be valuable for further research and clinical applications. Its design allows for straightforward adaptation to other treatment sites. Another advantage is its flexibility: the model parameters can easily be adjusted, facilitating future refinement as more clinical and biological data become available. Furthermore, the model can be used clinically for comparative dosimetric analysis, such as model-based selection for proton or photon therapy. In the Netherlands, a model-based approach is already established for indications like head-and-neck cancer, where both photon and proton therapy plans are created and evaluated based on normal tissue complication probability models (Langendijk *et al* 2013, 2021). Patients are selected for proton therapy when a clinically meaningful benefit is predicted.

While the model could aid in future efforts to spare the immune system, some limitations must be acknowledged and opportunities for further research should be explored. Firstly, the model focuses on lymphocytes in general, however, there are many subsets of lymphocytes and other immune cells, with different characteristics. The model can be tailored to a specific subset of lymphocytes, but the data on

the parameters are limited. Additionally, clinical validation of these findings is essential to establish their relevance, applicability, and accurateness. Future research should include a comparison between modeled lymphocyte counts and *in vivo* measured lymphocyte counts. With this comparison, the model can be fitted and the accuracy of the lymphocyte count prediction can be tested to increase its clinical utility. Furthermore, the apoptosis and production rates of lymphocytes are important for accurately modeling post-treatment recovery, but these parameters are not yet well researched. In our ongoing phase-II study comparing VMAT and IMPT for LACC blood samples are collected at 3 and 12 months post-treatment. This could quantify these rates and refine the recovery modeling. Another limitation of our model is that lymphocytes are assigned to a fixed compartment at a single reference time point, and this assignment is assumed constant throughout the beam-on period. Transitions between compartments during irradiation are not incorporated into dose estimation. This simplification may lead to either over- or underestimation of the actual dose. Future refinements could address this by modeling compartmental transitions during beam-on time. Additionally, the model does not account for the effects of chemotherapy on lymphocyte dynamics and depletion. For the dose prediction to lymphocytes, the effect of chemotherapy is not directly relevant, however, it significantly impacts lymphocyte counts (Stahnke *et al* 2001, Bazan *et al* 2013, Chu-Yuan *et al* 2013). Moreover, several biological responses to radiation and lymphocyte depletion were not included in our model, such as radiation-induced bone marrow suppression and lymphocyte recovery mechanisms triggered post-depletion, which may influence long-term lymphocyte levels. Another uncertainty that may influence these long-term levels are the parameters associated with the long-residence lymphocytes, since the exact proportion of tissue-resident lymphocytes and their transition dynamics are not quantitatively established in the literature. We incorporated this concept following consultations with experts in immunology and hematology. They agreed that modeling tissue-resident lymphocytes provides a more realistic representation of lymphocyte dynamics, consistent with the approach of Jin *et al* (2020). Finally, recent evidence suggests that the thymus retains active properties in the lymphatic system in adults when needed which is not included in our model (Chaudhry *et al* 2016, Kooshesh *et al* 2023, Taylor 2023). By addressing these limitations, the model can be refined and its predictive power improved.

In this study, a compartmental model was developed to simulate lymphocyte dynamics and predict the impact of EBRT on lymphocyte dose and survival in the treatment of LACC. By enabling lymphocyte count prediction at individual patient level, immune-sparing strategies can be evaluated and compared for LACC patients. The findings show the potential of proton therapy for sparing lymphocytes compared to photon therapy, thereby reducing RIL and potentially improving patient outcomes. With further improvements and clinical validation, this model could become a valuable tool for optimizing treatment planning, minimizing RIL, and enhancing the quality of care for patients undergoing radiotherapy.

Data availability statement

The data cannot be made publicly available upon publication due to legal restrictions preventing unrestricted public distribution. The data that support the findings of this study are available upon reasonable request from the authors.

Funding statement

This research was in part funded by a research grant of Varian Medical Systems, Inc. a Siemens Healthineers Company, Grant Number 2019 008.

Ethical statement

Written informed consent was obtained for all patients. This study was approved by the Medical Ethics Committee of Erasmus MC (Reference Number MEC 18-1363). The research was conducted in accordance with the principles embodied in the Declaration of Helsinki and the local statutory requirements.

Appendix A. Derivation effective average residence time $\left\langle t_{\mathrm{eff},i}^{\mathrm{S,L}} \right\rangle$

The average effective residence time for long and short-residing lymphocytes $\langle t_{\mathrm{eff},i}^{\mathrm{S,L}} \rangle$ is the expected time a lymphocyte remains in compartment i before either transitioning or undergoing apoptosis:

$$\langle t_{\mathrm{eff},i}^{\mathrm{S,L}} \rangle = \int_0^\infty \mathrm{d}t\, t q_i^{\mathrm{S,L}}(t)\,, \tag{A.1}$$

where $q_i(t)$ is the PDF of the time-to-removal. $q(t)$ can be derived by first defining the survival functions (probabilities of not having left/died before t), namely $S_i^{\mathrm{S,L}}(t) = \int_t^\infty \mathrm{d}t' p_i^{\mathrm{S,L}}(t')$ and $S^{\mathrm{ap}}(t) = \int_t^\infty \mathrm{d}t' p^{\mathrm{ap}}(t')$, where $p_i^{\mathrm{S,L}}$ and $p^{\mathrm{ap}}(t')$ are the PDFs for leaving compartment i or undergoing apoptosis.

In our model, transition and apoptosis times are independent, therefore, the overall survival before removal is the product of the two cause-specific survivals:

$$S_{\mathrm{re},i}^{\mathrm{S,L}}(t) = S_i^{\mathrm{S,L}}(t)\; S^{\mathrm{ap}}(t)\,. \tag{A.2}$$

The removal-time PDF $q(t)$ is then

$$q_i^{\mathrm{S,L}}(t) = -\frac{\mathrm{d}}{\mathrm{d}t} S_{\mathrm{re},i}^{\mathrm{S,L}}(t) \tag{A.3}$$

$$= p^{\mathrm{ap}}(t)\, S_i^{\mathrm{S,L}}(t) + p_i^{\mathrm{S,L}}(t)\, S^{\mathrm{ap}}(t)\,. \tag{A.4}$$

Substituting it all into equation (A.1) and using the definition for $p_i^{\mathrm{S,L}}(t)$ and $p^{\mathrm{ap}}(t)$ defined in equations (2) and (3) results in an expression for the average effective residence time for long and short-residing lymphocytes:

$$\langle t_{\mathrm{eff},i}^{\mathrm{S,L}} \rangle = \int_0^\infty \mathrm{d}t\, t \left(p_i^{\mathrm{S,L}}(t) \int_t^\infty \mathrm{d}t'\, p^{\mathrm{ap}}(t') + p^{\mathrm{ap}}(t') \int_t^\infty \mathrm{d}t'\, p_i^{\mathrm{S,L}}(t') \right) \tag{A.5}$$

$$= \int_0^\infty \mathrm{d}t\, t \left(\frac{\pi t}{2\langle t_i^{\mathrm{S,L}} \rangle^2}\, \mathrm{e}^{-k^{\mathrm{ap}} t - \frac{\pi t^2}{4\langle t_i^{\mathrm{S,L}} \rangle^2}} + k^{\mathrm{ap}}\, \mathrm{e}^{-k^{\mathrm{ap}} t - \frac{\pi t^2}{4\langle t_i^{\mathrm{S,L}} \rangle^2}} \right). \tag{A.6}$$

Appendix B. Derivation short-residing weight w_i^{S}

From literature, we obtained the fraction of lymphocytes that is long residing and short residing in a compartment in equilibrium. This fraction for short residing lymphocytes f_i^{S} can be defined as:

$$f_i^{\mathrm{S}} = \frac{N_i^{\mathrm{S}}}{N_i^{\mathrm{L}} + N_i^{\mathrm{S}}}, \tag{B.1}$$

where N_i^{S} and N_i^{L} are the number of short and long residing lymphocytes in compartment i. At equilibrium, the number of lymphocytes flowing in the compartment per unit time is equal to the number of lymphocytes leaving the compartment. The number of short- and long-residing lymphocytes in the compartment at equilibrium depends on both the probability of a lymphocytes becoming short- or long-residing and the mean effective residence times of the short- and long-residing lymphocytes. The steady-state number of lymphocytes in each compartment is given by the rate of inflow multiplied by the average effective residence time,

$$N_i^{\mathrm{S}} = \text{inflow rate} \times w_i^{\mathrm{S}} \times \langle t_{\mathrm{eff},i}^{\mathrm{S}} \rangle, \tag{B.2}$$

$$N_i^{\mathrm{L}} = \text{inflow rate} \times \left(1 - w_i^{\mathrm{S}}\right) \times \langle t_{\mathrm{eff},i}^{\mathrm{L}} \rangle, \tag{B.3}$$

$$N_i = N_i^{\mathrm{L}} + N_i^{\mathrm{S}} \tag{B.4}$$

$$= \text{inflow rate} \times \langle t_{\mathrm{eff},i} \rangle, \tag{B.5}$$

where $\langle t_{\mathrm{eff},i}^{\mathrm{S}} \rangle$ and $\langle t_{\mathrm{eff},i}^{\mathrm{L}} \rangle$ are the effective average residence time for the short and long-residing lymphocytes defined in equations (4). Substituting equation (B.2) and (B.5) into equation (B.1) results in

$$f_i^{\mathrm{S}} = \frac{w_i^{\mathrm{S}} \langle t_{\mathrm{eff},i}^{\mathrm{S}} \rangle}{\langle t_{\mathrm{eff},i} \rangle}. \tag{B.6}$$

The weight w_i^S can be solved by using $\langle t_{\text{eff},i}\rangle = \langle t^S_{\text{eff},i}\rangle w_i^S + \langle t^L_{\text{eff},i}\rangle(1-w_i^S)$ and solving equation (B.6) for w_i^S:

$$w_i^S = \frac{f_i^S \langle t^L_{\text{eff},i}\rangle}{\left(1-f_i^S\right)\langle t^S_{\text{eff},i}\rangle + f_i^S \langle t^L_{\text{eff},i}\rangle}. \tag{B.7}$$

Appendix C. Flow equations

In equation (7), the equilibrium equation for the number of lymphocytes in compartment i is given. This equation can be written down in vector notation as:

$$0 = \boldsymbol{K}\boldsymbol{N} + \boldsymbol{Q}. \tag{C.1}$$

In our model $\boldsymbol{N} = (N_B, N_{BM}, N_S, N_{LN}, N_{OT}, N_{Sk}, N_I)$, $\boldsymbol{Q} = (0, Q, Q, Q, 0, 0, 0)$, and:

$$\boldsymbol{K} = \begin{bmatrix} -k_1^{re} & k_2^{re}-k^{ap} & k_3^{re}-k^{ap} & k_4^{re}-k^{ap} & 0 & 0 & 0 \\ a_{12}\left(k_1^{re}-k^{ap}\right) & -k_2^{re} & 0 & 0 & 0 & 0 & 0 \\ a_{13}\left(k_1^{re}-k^{ap}\right) & 0 & -k_3^{re} & 0 & 0 & 0 & 0 \\ a_{14}\left(k_1^{re}-k^{ap}\right) & 0 & 0 & -k_4^{re} & k_5^{re}-k^{ap} & k_6^{re}-k^{ap} & k_7^{re}-k^{ap} \\ a_{15}\left(k_1^{re}-k^{ap}\right) & 0 & 0 & 0 & -k_5^{re} & 0 & 0 \\ a_{16}\left(k_1^{re}-k^{ap}\right) & 0 & 0 & 0 & 0 & -k_6^{re} & 0 \\ a_{17}\left(k_1^{re}-k^{ap}\right) & 0 & 0 & 0 & 0 & 0 & -k_7^{re} \end{bmatrix}$$

For notational simplicity, in this appendix we index compartments as $i \in \{1,2,\ldots,7\}$, corresponding to $i \in \{B, BM, Sp, LN, OT, Sk, I\}$, respectively.

We can derive the following seven constraints to adhere to the equilibrium state:

$$3Q = k^{ap} N_{tot}, \tag{3.2a}$$

$$a_{17} = 1 - a_{12} - a_{13} - a_{14} - a_{15} - a_{16}, \tag{3.2b}$$

$$k_i^{re} = \left(k_1^{re}-k^{ap}\right) a_{1i} \frac{N_1}{N_i} + d\frac{N_{tot}}{3N_i} \text{for } i = \{2,3\}, \tag{3.2c}$$

$$k_4^{re} = \left(k_1^{re}-k^{ap}\right)\left(1-a_{12}-a_{13}\right)\frac{N_1}{N_4} - k^{ap}\frac{\frac{1}{3}N_{tot}-N_5-N_6-N_7}{N_4}, \tag{3.2d}$$

$$k_i^{re} = \left(k_1^{re}-k^{ap}\right) a_{1i} \frac{N_1}{N_i} \text{for } i = \{5,6\}, \tag{3.2e}$$

With these constraints, seven parameters can be written as a function of the other parameters. These are used to impose the equilibrium constraints in our model.

Appendix D. Input parameters

This appendix provides explanation for the reference values of the parameters used in the model, along with the corresponding references. The values for most parameters are obtained from literature. For parameters that lacked reported values, educated guesses were made based on analogous parameters in the literature.

D.1. Number of lymphocytes in equilibrium N_i^{eq}

The parameter N_i^{eq} denotes the number of lymphocytes in compartment i in equilibrium. The values for these parameters were obtained from Trepel (1974). The model of Ford (1979), that we mainly use for our compartment model, applied these values to some extent. In our model, the lymphocytes in the thymus were not included as this organ is only marginally involved in the circulation of the lymphocytes in adults (Murray *et al* 2003, Blum and Pabst 2007). The number of lymphocytes in the blood, lymph nodes, spleen and bone marrow were $1\cdot10^{10}$, $19\cdot10^{10}$, $7\cdot10^{10}$, and $5\cdot10^{9}$ respectively (Trepel 1974). The number of lymphocytes in the intestines consisted of $3\cdot10^{10}$ in the intestinal mucosa and $2\cdot10^{10}$ in the lymphoid tissue of the gut, mainly the Peyer's patches. The other tissue in the article of Trepel (1974) consisted of $4\cdot10^{10}$ lymphocytes: $3\cdot10^{10}$ in the mucosa of the respiratory tract and $1\cdot10^{9}$ in the rest of the body. Furthermore, the number of lymphocytes in the skin was $2\cdot10^{10}$ Clark *et al* (2006).

D.2. Average residence time for short-residing lymphocytes $\langle t_i^S \rangle$

The average residence times for the short-residing lymphocytes $\langle t_i^S \rangle$ for the lymph nodes, spleen, and bone marrow are 16.5 h, 4.5 h, and 2.5 h (Rannie and Ford 1978, Ford 1979). The exact average short residence time for the intestines, skin, and other non-lymphoid tissue is not stated in these articles, however, it is stated that the lymphocytes return to the lymph nodes after these organs 'within a few hours' (Ford 1979). Therefore, we have put these values to 8 h, which is the average of the short-residence time of the lymph nodes, spleen, and bone marrow. For the blood compartment, $50 \cdot 10^{10}$ lymphocytes traffic in and out of the blood per day and the number of lymphocytes on a given moment is $1 \cdot 10^{10}$, therefore the average residence time of a lymphocyte in the blood is approximately 0.5 h (Westermann and Pabst 1992).

D.3. Average residence time for long-residing lymphocytes $\langle t_i^L \rangle$

The average residence time for long-residing lymphocytes $\langle t_i^L \rangle$ is not well-documented in the literature. To account for this, we have estimated the value to be 90 days (3 months) based on biological reasoning and the expectation that long-residing lymphocytes remain in specific compartments significantly longer than short-residing lymphocytes.

Although the exact value of $\langle t_i^L \rangle$ could vary, its influence on the model is minimal within the context of our simulation, as the treatment duration is only 35 days. Since the residence time far exceeds the treatment duration, variations in this parameter have a small effects on the model's dynamics during the treatment period.

D.4. The probability of a lymphocyte flowing from compartment i to j, a_{ij}

After a lymphocyte leaves the blood, 90% enters the lymph nodes, spleen, or bone marrow (Rannie and Ford 1978, Ford 1979). More specifically, 55%, 20%, and 15% enters the lymph nodes, spleen, and bone marrow. Furthermore, 2% enters the intestines and 8% enters the other tissues according to the study of Ford (1979). However, in this study the Peyer's patches are taken as part of the lymph nodes and in our model it is part of the intestines compartment. To correct for this, we reduced the percentage of lymphocytes that enters the lymph nodes to 18% and increase the number that enters the intestines to 4%. We are left with 8% for the other tissue and skin, however, the study of Ford (1979) does not include the skin as a compartment, such that we had to estimate a distribution. In our model, the initial values for the percentage that enters the skin was 3% and the other tissue compartment 5%.

D.5. Fraction of lymphocytes that is short-residing in equilibrium f_i^S

The fraction of lymphocytes that is short-residing in equilibrium f_i^S is not directly available in the literature. While there are studies discussing the presence of non-circulating lymphocytes in the skin (Clark *et al* 2006) and tissue-residing lymphocytes in non-lymphoid organs (Sathaliyawala *et al* 2013, Steinert *et al* 2015, Mackay and Kallies 2017), these focus on non-lymphoid organs and on specific subsets of lymphocytes rather than providing quantitative estimates for all compartments.

To parameterize f_i^S, we considered the framework described in Jin *et al* (2020), which tested 5%, 10%, and 20% of lymphocytes to be short residing (referred to as non-circulating) in the different compartments, except for blood where they assume a value of 100% short residing. We used 20% for the compartments except blood compartment. For this last compartment, our model incorporated additional data indicating that approximately 40% of lymphocytes in the blood never leave this compartment (Young *et al* 1997).

D.6. The apoptosis rate k^{ap} and production Q

There is a wide variability in the apoptosis rate and proliferation between the different lymphocyte subsets. In the study of Sender and Milo (2021), several studies were combined to create an overview of the distribution and proliferation of different lymphocyte subsets. In table D1, a concise overview of their findings that we used to estimate the average proliferation of a lymphocyte is shown. The proliferation of the NK-cells is obtained from the study of Lutz *et al* (2011). Combining the values in this overview results in an average lifespan of 977 d which corresponds to an apoptosis rate of $k^{ap} = 4.3 \cdot 10^{-5}\,\mathrm{h}^{-1}$. Using the equilibrium equation for lymphocyte production and apoptosis (equation (3.2)), the production, Q, is determined to be $Q = 6.1 \cdot 10^{6}\ \mathrm{h}^{-1}$.

Table D1. Distribution, lifespan and proliferation rate per type of lymphocytes based on data of Sender and Milo (2021) and Lutz *et al* (2011).

Type	Subtype	Function	Lifespan (d)	Apoptosis rate (h^{-1})
T (65%)	CD4+ (60%)	Naive (46%)	2500	1.67×10^{-5}
		Memory (50%)	167	2.50×10^{-4}
	CD8+ (30%)	Naive (41%)	3333	1.25×10^{-5}
		Memory (41%)	189	2.20×10^{-4}
B (30%)			128	3.26×10^{-4}
NK (5%)			13.5	3.08×10^{-3}

ORCID iDs

Sander C Kuipers 0000-0002-8844-6749
Anouk Corbeau 0000-0003-3919-5135
Stephanie M de Boer 0000-0002-8454-1597

References

Bazan J G, Luxton G, Kozak M M, Anderson E M, Hancock S L, Kapp D S, Kidd E A, Koong A C and Chang D T 2013 Impact of chemotherapy on normal tissue complication probability models of acute hematologic toxicity in patients receiving pelvic intensity modulated radiation therapy *Int. J. Radiat. Oncol. Biol. Phys.* **87** 983–91

Beekman C, Carrasco-Rojas N, Withrow J, Dawson R, Bolch W E and Paganetti H 2025 Radiation-induced lymphopenia: in silico replications of preclinical studies suggest importance of dose to lymphoid organs *Int. J. Radiat. Oncol. Biol. Phys.* **123** 550–62

Blum K S and Pabst R 2007 Lymphocyte numbers and subsets in the human blood *Immunol. Lett.* **108** 45–51

Chaudhry M S, Velardi E, Dudakov J A and van den Brink M R 2016 Thymus: the next (re)generation *Immunol. Rev.* **271** 56–71

Chu-Yuan H, Jing P, Yi-Sheng W, He-Ping P, Hui Y, Chu-Xiong Z, Guo-Jian L and Guo-Qiang W 2013 The impact of chemotherapy-associated neutrophil/ lymphocyte counts on prognosis of adjuvant chemotherapy in colorectal cancer *BMC Cancer* **13** 1–10

Chung H C *et al* 2019 Efficacy and safety of pembrolizumab in previously treated advanced cervical cancer: results from the phase II KEYNOTE-158 study *J. Clin. Oncol.* **37** 1470–8

Cibula D, Pötter R, Planchamp F, Avall-Lundqvist E, Fischerova D, Haie-Meder C, Köhler C, Landoni F, Lax S and Lindegaard J C 2018 The European society of gynaecological oncology/European society for radiotherapy and oncology/European society of pathology guidelines for the management of patients with cervical cancer *Virchows Arch.* **472** 919–36

Clark R A, Chong B, Mirchandani N, Brinster N K, Yamanaka K-I, Dowgiert R K and Kupper T S 2006 The vast majority of CLA+ T cells are resident in normal skin *J. Immunol.* **176** 4431–9

Colombo N *et al* 2021 Pembrolizumab for persistent, recurrent, or metastatic cervical cancer *New Engl. J. Med.* **385** 1856–67

Corbeau A *et al* 2021b PROTECT: prospective phase-II-trial evaluating adaptive proton therapy for cervical cancer to reduce the impact on morbidity and the immune system *Cancers* **13** 5179

Corbeau A, Kuipers S C, de Boer S M, Horeweg N, Hoogeman M S, Godart J and Nout R A 2021a Correlations between bone marrow radiation dose and hematologic toxicity in locally advanced cervical cancer patients receiving chemoradiation with cisplatin: a systematic review *Radiother. Oncol.* **164** 128–37

Cortiula F *et al* 2024 Proton and photon radiotherapy in stage III NSCLC: effects on hematological toxicity and adjuvant immune therapy *Radiother. Oncol.* **190** 110019

Damen P J J, Kroese T E, van Hillegersberg R, Schuit E, Peters M, Verhoeff J J C, Lin S H and van Rossum P S N 2021 The influence of severe radiation-induced lymphopenia on overall survival in solid tumors: a systematic review and meta-analysis *Int. J. Radiat. Oncol. Biol. Phys.* **111** 936–48

de Kermenguy F *et al* 2024 LymphoDose: a lymphocyte dose estimation framework—application to brain radiotherapy *Phys. Med. Biol.* **69** 105009

Ellis R E 1961 The distribution of active bone marrow in the adult *Phys. Med. Biol.* **5** 255

Fang P, Shiraishi Y, Verma V, Jiang W, Song J, Hobbs B P and Lin S H 2017 Lymphocyte-sparing effect of proton therapy in patients with esophageal cancer treated with definitive chemoradiation *Int. J. Part. Therapy* **4** 23–32

Ford W L 1979 Lymphocytes. 3. Distribution. Distribution of lymphocytes in health *J. Clin. Pathol.* **13** 63

Gort E M, Beukema J C, Matysiak W, Sijtsema N M, Aluwini S, Langendijk J A, Both S and Brouwer C L 2021 Inter-fraction motion robustness and organ sparing potential of proton therapy for cervical cancer *Radiother. Oncol.* **154** 194–200

Horeweg N, Creutzberg C L, Rijkmans E C, Laman M S, Velema L A, Coen V L M A, Stam T C, Kerkhof E M, Kroep J R and de Kroon C D 2019 Efficacy and toxicity of chemoradiation with image-guided adaptive brachytherapy for locally advanced cervical cancer *Int. J. Gynecol. Cancer* **29** 257–65

Huang J, Gu F, Ji T, Zhao J and Li G 2020 Pelvic bone marrow sparing intensity modulated radiotherapy reduces the incidence of the hematologic toxicity of patients with cervical cancer receiving concurrent chemoradiotherapy: a single-center prospective randomized controlled trial *Radiat. Oncol.* **15** 180

Jin J-Y *et al* 2020 A framework for modeling radiation induced lymphopenia in radiotherapy *Radiother. Oncol.* **144** 105–13

Jin J *et al* 2017 Higher radiation dose to immune system is correlated with poorer survival in patients with stage III non–small cell lung cancer: a secondary study of a phase 3 cooperative group trial (NRG Oncology RTOG 0617) *Int. J. Radiat. Oncol. Biol. Phys.* **99** S151–2

Kim C H *et al* 2020 ICRP publication 145: adult mesh-type reference computational phantoms *Ann. ICRP* **49** 13–201

Kim N, Noh J M, Lee W, Park B, Park H, Park J Y and Pyo H 2021 Proton beam therapy reduces the risk of severe radiation-induced lymphopenia during chemoradiotherapy for locally advanced non-small cell lung cancer: a comparative analysis of proton versus photon therapy *Radiother. Oncol.* **156** 166–73

Kooshesh K A, Foy B H, Sykes D B, Gustafsson K and Scadden D T 2023 Health consequences of thymus removal in adults *New Engl. J. Med.* **389** 406–17
Kuipers S, Godart J, Corbeau A, Breedveld S, Mens J, de Boer S, Nout R and Hoogeman M 2024 Dosimetric impact of bone marrow sparing for robustly optimized IMPT for locally advanced cervical cancer *Radiother. Oncol.* **195** 110222
Kuipers S, Godart J, Corbeau A, Sharfo A W, Breedveld S, Mens J W, de Boer S, Nout R and Hoogeman M 2023 The impact of bone marrow sparing on organs at risk dose for cervical cancer: a Pareto front analysis *Front. Oncol.* **13** 1138433
Langendijk J A *et al* 2021 National protocol for model-based selection for proton therapy in head and neck cancer *Int. J. Part. Therapy* **8** 354–65
Langendijk J A, Lambin P, De Ruysscher D, Widder J, Bos M and Verheij M 2013 Selection of patients for radiotherapy with protons aiming at reduction of side effects: the model-based approach *Radiother. Oncol.* **107** 267–73
Li Y *et al* 2023 Proton and carbon ion radiation therapy decreased severe lymphopenia by reducing thoracic vertebra and aortic doses in non-small cell lung cancer versus intensity modulated radiation therapy *Int. J. Radiat. Oncol. Biol. Phys.* **116** 579–89
Lorusso D *et al* 2024 Pembrolizumab or placebo with chemoradiotherapy followed by pembrolizumab or placebo for newly diagnosed, high-risk, locally advanced cervical cancer (ENGOT-cx11/GOG-3047/KEYNOTE-A18): overall survival results from a randomised, double-blind, placebo-controlled, phase 3 trial *Lancet* **404** 1321–32
Lutz C T, Karapetyan A, Al-Attar A, Shelton B J, Holt K J, Tucker J H and Presnell S R 2011 Human NK cells proliferate and die *In Vivo* more rapidly than T cells in healthy young and elderly adults *J. Immunol.* **186** 4590–8
Mackay L K and Kallies A 2017 Transcriptional regulation of tissue-resident lymphocytes *Trends Immunol.* **38** 94–103
Mohan R *et al* 2021 Proton therapy reduces the likelihood of high-grade radiation-induced lymphopenia in glioblastoma patients: phase II randomized study of protons vs photons *Neuro-Oncology* **23** 284–94
Monk B J *et al* 2023a First-line pembrolizumab + chemotherapy versus placebo + chemotherapy for persistent, recurrent, or metastatic cervical cancer: final overall survival results of KEYNOTE-826 *J. Clin. Oncol.* **41** 5505–11
Monk B J *et al* 2023b Durvalumab versus placebo with chemoradiotherapy for locally advanced cervical cancer (CALLA): a randomised, double-blind, phase 3 trial *Lancet Oncol.* **24** 1334–48
Murray J M, Kaufmann G R, Hodgkin P D, Lewin S R, Kelleher A D, Davenport M P and Zaunders J J 2003 Naive T cells are maintained by thymic output in early ages but by proliferation without phenotypic change after age twenty *Immunol. Cell Biol.* **81** 487–95
Paganetti H 2023 A review on lymphocyte radiosensitivity and its impact on radiotherapy *Front. Oncol.* **13** 1201500
Page S M and Rollins M D 2019 *Pharmacology and Physiology for Anesthesia* (Elsevier) pp 732–51
Panici P B, Scambia G, Baiocchi G, Matonti G, Capelli A and Mancuso S 1992 Anatomical study of para-aortic and pelvic lymph nodes in gynecologic malignancies *Obstetr. Gynecol.* **79** 498–502
Pötter R, Tanderup K, Kirisits C, de Leeuw A, Kirchheiner K, Nout R, Tan L T, Haie-Meder C, Mahantshetty U and Segedin B 2018 The EMBRACE II study: the outcome and prospect of two decades of evolution within the GEC-ESTRO GYN working group and the EMBRACE studies *Clin. Transl. Radiat. Oncol.* **9** 48–60
Pötter R, Tanderup K, Schmid M P, Jürgenliemk-Schulz I, Haie-Meder C, Fokdal L U, Sturdza A E, Hoskin P, Mahantshetty U and Segedin B 2021 MRI-guided adaptive brachytherapy in locally advanced cervical cancer (EMBRACE-I): a multicentre prospective cohort study *Lancet Oncol.* **22** 538–47
Qatarneh S M, Kiricuta I-C, Brahme A, Tiede U and Lind B K 2006 Three-dimensional atlas of lymph node topography based on the visible human data set *Anatom. Rec. B* **289** 98–111
Rannie G and Ford W 1978 Recirculation of lymphocytes: its role in implementing immune responses in the skin *Lymphology* **11** 193–201
Routman D M *et al* 2019 A comparison of grade 4 lymphopenia with proton versus photon radiation therapy for esophageal cancer *Adv. Radiat. Oncol.* **4** 63–69
Sathaliyawala T, Kubota M, Yudanin N, Turner D, Camp P, Thome J J C, Bickham K L, Lerner H, Goldstein M and Sykes M 2013 Distribution and compartmentalization of human circulating and tissue-resident memory T cell subsets *Immunity* **38** 187–97
Sender R and Milo R 2021 The distribution of cellular turnover in the human body *Nat. Med.* **27** 45–48
Shin J, Xing S, McCullum L, Hammi A, Pursley J, Correa C A, Withrow J, Domal S, Bolch W and Paganetti H 2021 HEDOS—a computational tool to assess radiation dose to circulating blood cells during external beam radiotherapy based on whole-body blood flow simulations *Phys. Med. Biol.* **66** 164001
Shiraishi Y *et al* 2018 Severe lymphopenia during neoadjuvant chemoradiation for esophageal cancer: a propensity matched analysis of the relative risk of proton versus photon-based radiation therapy *Radiother. Oncol.* **128** 154–60
Stahnke K, Fulda S, Friesen C, Strauß G and Debatin K M 2001 Activation of apoptosis pathways in peripheral blood lymphocytes by *in vivo* chemotherapy *Blood* **98** 3066–73
Steinert E M, Schenkel J M, Fraser K A, Beura L K, Manlove L S, Igyártó B Z, Southern P J and Masopust D 2015 Quantifying memory CD8 T cells reveals regionalization of immunosurveillance *Cell* **161** 737–49
Taylor N 2023 The thymus - not a graveyard after all, even in adults? *N. Engl. J. Med.* **389** 470–1
Trepel F 1974 Zahl und Verteilung der Lymphocyten des Menschen. Eine kritische Analyse *Klin. Wochenschr.* **52** 511
Westermann J and Pabst R 1992 Distribution of lymphocyte subsets and natural killer cells in the human body *Clin. Invest.* **70** 539–44
Wu E S, Oduyebo T, Cobb L P, Cholakian D, Kong X, Fader A N, Levinson K L, Tanner Iii E J, Stone R L and Piotrowski A 2016 Lymphopenia and its association with survival in patients with locally advanced cervical cancer *Gynecol. Oncol.* **140** 76–82
Young A J, Marston W L, Dessing M, Dudler L and Hein W R 1997 Distinct recirculating and non-recirculating B-lymphocyte pools in the peripheral blood are defined by coordinated expression of CD21 and L-Selectin *Blood* **90** 4865–75